

Hot, dense HeII outflows during the 2017 outburst of the X-ray transient Swift J1357.2-0933

Phil Charles,¹  James H. Matthews,² David A.H. Buckley,³ Poshak Gandhi,¹ Enrico Kotze,^{3,4} and John Paice^{1,5}

¹Department of Physics & Astronomy, University of Southampton, Southampton SO17 1BJ, UK

²Astrophysics, Department of Physics, University of Oxford, Keble Road, Oxford OX1 3RH, UK

³South African Astronomical Observatory, P.O.Box 9, Observatory, 7935, South Africa

⁴Southern African Large Telescope, P.O.Box 9, Observatory, 7935, South Africa

⁵Inter-University Centre for Astronomy & Astrophysics, Post Box 4, Ganeshkhind, Pune-411007, India

21 March 2022

ABSTRACT

Time-resolved SALT spectra of the short-period, dipping X-ray transient, Swift J1357.2-0933, during its 2017 outburst has revealed broad Balmer and HeII $\lambda 4686$ absorption features, blue-shifted by ~ 600 km s $^{-1}$. Remarkably these features are also variable on the ~ 500 s dipping period, indicating their likely association with structure in the inner accretion disc. We interpret this as arising in a dense, hot ($\gtrsim 30,000$ K) outflowing wind seen at very high inclination, and draw comparisons with other accretion disc corona sources. We argue against previous distance estimates of 1.5kpc and favour a value $\gtrsim 6$ kpc, implying an X-ray luminosity $L_X \gtrsim 4 \times 10^{36}$ erg s $^{-1}$. Hence it is *not* a very faint X-ray transient. Our preliminary 1D Monte-Carlo radiative transfer and photoionization calculations support this interpretation, as they imply a high intrinsic L_X , a column density $N_H \gtrsim 10^{24}$ cm $^{-2}$ and a low covering factor for the wind. Our study shows that Swift J1357.2-0933 is truly remarkable amongst the cohort of luminous, galactic X-ray binaries, showing the first example of HeII $\lambda 4686$ absorption, the first (and only) variable dip period and is possibly the first black hole ‘accretion disc corona’ candidate.

Key words: accretion, accretion discs – stars: black holes – X-rays: binaries

1 INTRODUCTION

The low-mass X-ray binary transients (XRTs) are short-period (usually ≤ 1 d) interacting binaries, where a compact object (neutron star, NS, or black hole, BH) accretes material from its low-mass donor via an accretion disc. Detected only during outburst we now know of ~ 50 such objects, of which $\sim 75\%$ contain BHs, the remainder NSs, based on their X-ray and other properties. These systems are outstanding laboratories for studying the late stages of stellar evolution, and determining fundamental properties of compact objects (see Charles & Coe 2006, Casares & Jonker 2014, and the Black-CAT (Corral-Santana et al. 2016) and WATCHDOG (Tetarenko et al. 2016) catalogues for more details). The great majority of Galactic XRTs are in or close to the galactic plane, and only a handful appear to be at high ($\sim 70^\circ$) inclination, and none are eclipsing. Furthermore, the last decade has seen an increase in those found at high latitude, one of which, Swift J1357.2-0933 (hereafter J1357.2) is the subject of this paper.

Discovered by Swift/BAT in 2011, J1357.2 peaked at a very low $L_X \sim 10^{35}$ erg s $^{-1}$, when compared to other BH XRTs, assuming

a ~ 1.5 kpc) location (Armas Padilla & et al. 2014, and references therein). This estimate was based on the optical identification of a substantially brightened (~ 6 mags) counterpart (Rau et al. 2011), which had a very faint, red star at the same position on archival plates. The outburst declined exponentially in X-rays, and was undetectable within 6 months (Tetarenko et al. 2018). However, what drew attention to J1357.2 was the discovery (Corral-Santana et al. 2013, hereafter CS13) of periodic optical dipping. Such dipping has been seen before in other short-period LMXBs (e.g. A1916-05, see Homer et al. 2001), and is due to the raised disc rim caused by the stream-impact from the donor, thereby producing obscuration of the inner disc regions when viewed at high inclination. These dips therefore recur on the orbital period (usually \sim hours), but what was truly remarkable about J1357.2 was that, not only were the periodic dips recurring much too rapidly (\sim minutes) to be the binary period, but as the outburst progressed, the dip period was seen to lengthen. Such variable-periodic dipping had never been seen before (nor since) in any other system. It was interpreted by CS13 as being due to the gradual expansion of an inner torus in the disc, with associated structure (e.g. variable height) that led to the dipping. At any given time, the dipping period would be that associated with the Keplerian rotation of the torus at that radius.

* E-mail: p.a.charles@soton.ac.uk

Optical spectroscopy of J1357.2 during outburst revealed strong, double-peaked H and HeI emission-lines, typical of a high-inclination disc. Furthermore, CS13 found evidence for a 2.8 ± 0.3 h orbital period in their $H\alpha$ radial velocities, making it one of the shortest period systems amongst all the BH XRTs. This was refined by Mata Sánchez et al. (2015) who inferred $M_1 > 9.3 M_\odot$ and $q \sim 0.04$, strengthening its BH candidature. Such a short period would then imply a very low-mass donor, whose size CS13 suggested could be sufficiently small ($\leq 0.1 R_\odot$) that it would be permanently in the shadow of the accretion disc, thereby explaining the absence of X-ray or optical orbital modulations, even at a very high inclination.

Just 6 years after its discovery, J1357.2 produced a second outburst in 2017 (Drake & et al. 2017), and the dips were again present and varying in frequency as during 2011 (Paice et al. 2019, hereafter P19). Furthermore, simultaneous SALT/NTT-ULTRACAM photometry and NuSTAR observations revealed no X-ray counterpart to the dips (see also Beri et al. 2019), which unusually were shown to be blue, leading P19 to propose that they were caused by a moving, raised region within the inner disc that was obscuring a luminous, red emitting area. In addition to P19’s optical photometry, we also exploited the relative brightness of J1357.2 in outburst ($V=16$) to obtain SALT time-resolved spectra with the aim of searching for spectral signatures of the dips that could help explain their physical origin, and the resulting spectra are presented here. Obtained later in the outburst, when the dipping period was ~ 500 s, these results should be viewed in parallel with those reported by (Jiménez-Ibarra et al. 2019, hereafter JI19) taken a month earlier.

2 OBSERVATIONS AND DATA REDUCTION

We obtained medium-resolution spectroscopy of J1357.2 on 2017 April 28 (2×1400 s), 29 (4×600 s) and July 21 using the SALT Robert Stobie Spectrograph (RSS) and G0900 grating (Buckley et al. 2006). With the July 21 spectroscopy our aim was to temporally resolve the absorption dips, so we used RSS in Frame-Transfer mode, obtaining 31 100 s exposures (with no dead-time) during the SALT track. The dip period at this time was ~ 500 s (see P19). Combined with a 1.5 arcsec slit, all spectra covered the $\lambda\lambda 4100-7100$ range at a resolving power of ~ 1000 .

These data, plus associated arcs and bias frames, were pipeline-processed (Crawford et al. 2010), followed by cosmic-ray removal using the IRAF task L.A. Cosmic (Van Dokkum 2001) on the 2D image, and wavelength calibrated using standard IRAF (Tody 1986) routines. While SALT’s continuously varying entrance pupil precludes accurate flux calibration, these spectra have been divided by a suitable standard star (LTT4364: Hamuy et al. 1994) to remove instrumental response features. The July time-series average spectrum is shown in Figure 1, along with Apr 28/29 for comparison.

An indication of the variability present during the July SALT run (Figure 2) uses a nearby field star (SDSS J135716.43-093140.1) also on the slit for reference. Colour variations are shown by using the flux ratio in the blue and red RSS CCDs. There is clear variability on the dip timescale ($\sim 500-800$ s), and we note that the spectrum at time 1100 s is particularly blue.

The key spectral feature that is highly variable is the broad, blue-shifted (~ 600 km s $^{-1}$) HeII $\lambda 4686$ and Balmer absorption. These variations are highlighted in Fig. 3 which displays the 31 individual spectra as a grey-scale. The features are strongest in spectra 7, 12, 13 and 24, see Figure 4 zoomed-in on HeII/H β and $H\alpha$. Fitting single gaussians gives centroid blue-shifts of $10 \pm X$

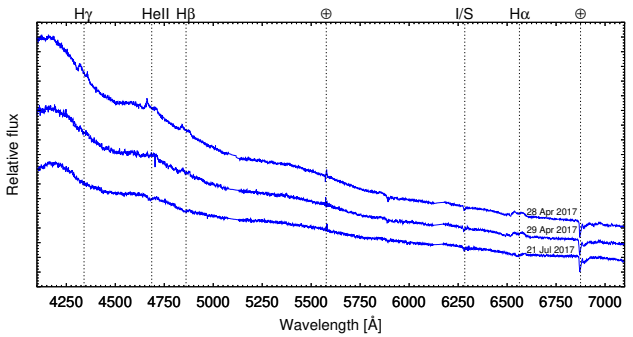


Figure 1. Mean SALT RSS spectra of J1357.2, with key spectral features marked with dotted lines, including the diffuse interstellar band at $\lambda 6283$. The April spectra are similar to those of CS13 with double-peaked HeII and Balmer emission profiles typical of a high-inclination disc. Terrestrial atmospheric features (OI, B-band) are marked \oplus .

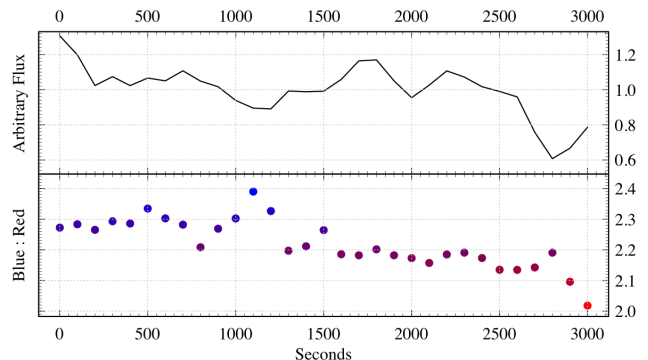


Figure 2. *Upper:* Light curve of J1357.2 (relative to its mean) from the July 21 RSS spectra by using a comparison star on the slit. *Lower:* Approximate blue/red colour variations from the total flux in the blue ($\lambda\lambda 4100-5100$) and red ($\lambda\lambda 6200-7100$) CCDs, relative to the same star.

\AA for HeII and $H\alpha$, corresponding to ≈ 600 km s $^{-1}$, and FWHM in the range 500-700 km s $^{-1}$. The maximum blueshift is around 1500 km s $^{-1}$ in HeII $\lambda 4686$ and $H\beta$, and even higher in $H\alpha$.

3 MODELLING AN UNUSUAL DISC WIND

Such a large blue-shift in J1357.2’s absorption features, also seen by JI19 a month earlier, is a *smoking gun* signal of outflowing material, presumably a disc wind. Spectral signatures (usually in the form of blue-shifted broad absorption lines [BALs] or P-Cygnus profiles) of outflowing material from accreting objects have regularly been seen at all wavelengths. Indeed, they appear ubiquitous, having been well-studied across the full mass spectrum, from cataclysmic variables (CVs) to supermassive BHs (see e.g. Matthews 2016, for a review). In X-ray binaries, equatorial disc winds are thought to be produced in the soft state as inferred from broad Fe xxv/xxvi absorption (Ponti et al. 2012). In addition, blue-shifted HeI and $H\alpha$ absorption has been detected in V404 Cyg (Casares et al. 1991; Muñoz-Darias et al. 2016; Muñoz-Darias et al. 2017; Mata Sánchez et al. 2018), V4641 Sgr (Muñoz-Darias et al. 2018), MAXI J1820+070 (Muñoz-Darias et al. 2019) and CVs (Kafka & Honeycutt 2004). Optically detected P-Cygni profiles indicate the

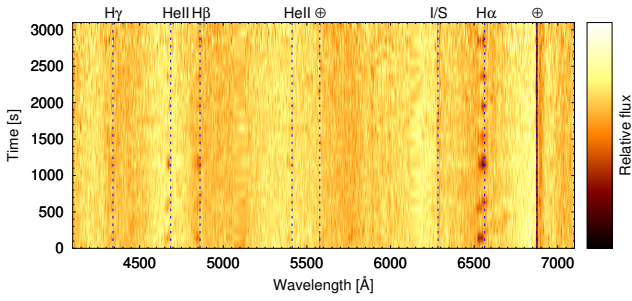


Figure 3. SALT time-series spectra of J1357.2 on 21 July 2017, displayed as a grey-scale with time increasing from bottom to top. Key spectral features are marked with dotted lines. Note in particular the strong variations in HeII $\lambda 4686$ and $H\beta$ that are associated with the dipping frequency.

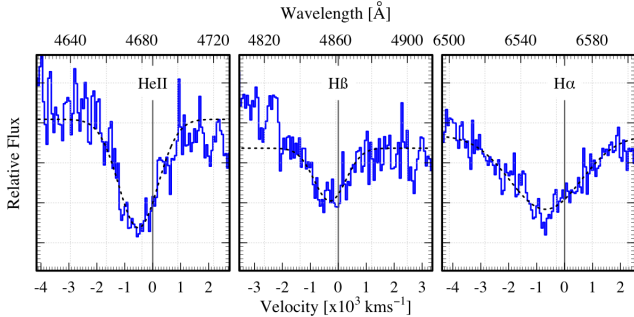


Figure 4. Zoomed sections of the mean of four SALT RSS spectra of J1357.2 on 2017 July 21, where HeII $\lambda 4686$, $H\beta$ and $H\alpha$ absorption features are strongest. Gaussian fits to the line profiles are shown, as are the velocities relative to rest wavelength.

presence of cooler ($\sim 10,000$ K) outflowing material compared to the X-ray wind detections, though the extent to which the two phenomena are related is not yet known.

3.1 Radiative Transfer Method and Model Setup

Modelling a disc wind in J1357.2 is challenging given the lack of constraining information about the outflow geometry and intrinsic radiation source. We assume that the outflow is photoionized by a central X-ray source and all heating sources are radiative, which may or may not be reasonable. For our modelling, we used a Monte Carlo radiative transfer code, confusingly known as `PYTHON` (see [Long & Knigge \(2002\)](#), with subsequent updates and testing described by [Sim et al. \(2005\)](#), [Higginbottom et al. \(2013\)](#) and [Matthews et al. \(2015\)](#)). The code first calculates the outflow's ionization and temperature structure, before computing the detailed spectrum from the converged model. We adopt the hybrid macro-atom approach to line transfer, described by [Matthews et al. \(2015\)](#), in which H and He are treated as macro-atoms according to the formalism of [Lucy \(2002, 2003\)](#), whereas metals are treated as ‘simple-atoms’. This is a well-tested technique that has been used to model line formation when there are large departures from LTE, such as in supernovae (e.g. [Kromer & Sim 2009](#)). Convergence criteria are described by [Long & Knigge \(2002\)](#) and, briefly, require that the electron temperature, T_e , has stopped changing significantly and that heating and cooling are closely balanced. The model spectra presented here come from models with 100% convergence, although some of the models

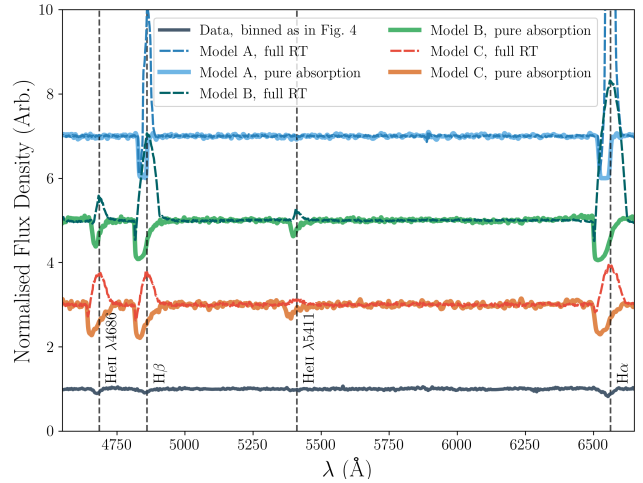


Figure 5. Continuum normalised model spectra, calculated with full radiative transfer and in the pure absorption limit, compared to observational data. We show three models that produced obvious HeII $\lambda 4686$ and/or Balmer absorption lines: Model A ($\dot{M}_{w,\text{iso}} = 10^{-7} M_\odot \text{ yr}^{-1}$, $L_{2-10} = 10^{35} \text{ erg s}^{-1}$, $\beta = 4$), Model B ($\dot{M}_{w,\text{iso}} = 10^{-6} M_\odot \text{ yr}^{-1}$, $L_{2-10} = 10^{36} \text{ erg s}^{-1}$, $\beta = 0.5$), and Model C ($\dot{M}_{w,\text{iso}} = 10^{-5} M_\odot \text{ yr}^{-1}$, $L_{2-10} = 10^{37} \text{ erg s}^{-1}$, $\beta = 0.5$). See text for details. For clarity, offsets of +6,+4 and +2 are applied to models A, B and C, respectively.

(12/54) in the simulation grid did not converge well. The poorly converged models were all at either the extreme low or high ionization end of the simulating grid, and the models in between allowed us to cover the region of parameter space where HeII $\lambda 4686$ first appeared and then disappeared. Nevertheless, further exploration of parameter space is merited.

Our 1D spherically-symmetric model uses 30 radial cells separated logarithmically (see [Matthews 2016](#)). The velocity at radius R is set according to a so-called β -law, $v(R) = v_0 + (v_\infty - v_0)[1 - (R_0/R)]^\beta$, where R_0 is the initial radius, v_0 and v_∞ the initial and terminal velocities and β governs the rate of acceleration. This velocity law is commonly used to model stellar winds (e.g. [Puls et al. 1996](#)), and, while it may not be correct, it gives an appropriate starting point. The density, $\rho(R)$, is calculated from the isotropic mass loss rate, $\dot{M}_{w,\text{iso}} = 4\pi R^2 \rho v$. The illuminating spectral energy distribution (SED) is $F_\nu \propto \nu^{-\alpha}$, with a low-frequency cutoff at $\nu_c = 10^{17} \text{ Hz}$ and 2-10 keV luminosity L_{2-10} . We conducted a small grid of simulations over the parameters L_{2-10} (from $10^{35} - 10^{37.5} \text{ erg s}^{-1}$ in steps of 0.5 dex), $\dot{M}_{w,\text{iso}}$ ($10^{-5}, 10^{-6}, 10^{-7} M_\odot \text{ yr}^{-1}$) and β (0.5, 1, 4). We fixed $\alpha = 0.8$, $v_0 = 100 \text{ km s}^{-1}$, $v_\infty = 3000 \text{ km s}^{-1}$ and set R_0 to the approximate radius at which the Keplerian period equals the dip period ($2 \times 10^{10} \text{ cm}$). Note that $\dot{M}_{w,\text{iso}}$ is not the true mass-loss rate, rather a normalisation of the flow density. The true rate will be significantly lower due to the covering factor of the wind.

3.2 Simulation Results

We find that a fraction (9 out of 54) of our models produce HeII $\lambda 4686$ absorption, appearing as P-Cygni profiles due to the model's spherical symmetry. Fig. 5 compares the data from Figure 4 with two spherical models from our simulations. For each model, we include the spectrum as calculated with full radiative transfer as well as in the pure absorption limit, where radiation packets are discarded once macro-atoms are activated. In the pure

absorption limit, the models show clear blue-shifted BALs in $H\alpha$, $H\beta$ and $HeII\lambda 4686$. In the full RT case, these absorption profiles are mostly swamped by emission, and, notably, the emission and absorption profiles do not sum to zero as would be expected from pure scattering lines in spherical symmetry. This indicates that there is a non-scattering contribution to the line source function. One interpretation of the pure absorption spectrum observed is that it is due to a low covering factor for the wind. The pure absorption model spectrum also shows much deeper absorption troughs compared to that observed, which could be due to partial covering of the optical continuum or emission lines from the wind partially filling in the troughs. The absorption troughs in both the models and the data show absorption redward of line centre. In the data, this might be caused by rotation. In the models, it is due to obscuration of the reprocessed continuum by the far side of the wind, since $v_c = 10^{17}\text{Hz}$ and the optical continuum is entirely produced by X-ray reprocessing. In models where $HeII\lambda 4686$ absorption is produced, this reprocessed continuum actually peaks in the UV and the soft X-rays are heavily absorbed by the wind, behaviour which is consistent with the findings of [Beri et al. \(2019\)](#) from UV and X-ray observations during the same outburst.

In our simulation grid, we required the following properties to produce $HeII\lambda 4686$ absorption: (i) $L_{2-10} \gtrsim 10^{36}\text{ erg s}^{-1}$; (ii) $\dot{M}_{w,\text{iso}} \gtrsim 10^{-6} M_\odot \text{ yr}^{-1}$, leading to maximum densities of $n_H \sim 10^{13-14} \text{ cm}^{-3}$ and column densities of $N_H \gtrsim 10^{24} \text{ cm}^{-2}$; (iii) corresponding ionization parameters of $\xi \sim 100$ and $T_e \approx 20,000 - 70,000\text{K}$. We found that models with lower L_{2-10} were under-ionized and only produced Balmer absorption or none at all (an example is shown in Fig. 5). Models with lower mass loss-rates did not have sufficient line opacity. The modelling results give us clues to the physical conditions in the outflow, but they should be interpreted with caution. For example, we may be limited by our imposed velocity law or geometry. In particular, in a 1D model there is only one route for X-rays to reach the outer parts of the wind, whereas we already know the X-ray source is not eclipsed and the absorption lines are phase dependent, which means that 2D and 3D radiative transfer effects *must* play a role. We therefore cannot draw robust constraints on parameters from this modelling. However, importantly, we have demonstrated that $HeII\lambda 4686$ absorption can be produced for reasonable system parameters and is suggestive of a relatively high intrinsic L_X , as well as a high density and a low covering factor for the outflow.

4 DISCUSSION

Our time-resolved spectroscopy of J1357.2 has revealed a hot spectral component that appears associated with the optical absorption dips. What is remarkable about this component is that it has $HeII\lambda 4686$ in absorption, a feature normally only seen in very hot stars (early O stars, [Walborn & Fitzpatrick 1990](#), and DO/DB white dwarfs, [Wesemael et al. 1993](#)). Yet the substantial blue-shift in all the strong absorption features is compelling evidence for associating them with an accretion disc wind, as modelled in the previous section, launched from a region which gradually moves out through the disc as the outburst progresses. Indeed we note that our observed blue-shift is significantly less than that seen by J119, as expected given the lower escape velocity at the larger radius. $HeII\lambda 4686$ absorption has never been seen in a disc wind before, although there is evidence in [Quimby et al. \(2007\)](#) and [Dessart et al. \(2008\)](#) for its presence during the shock break-out phase in Type IIP supernovae,

while $HeII\lambda 1640$ wind features have been seen in FUV spectra of CVs ([Long et al. 1991](#); [Hoare 1994](#)).

Amongst the now several hundred LMXBs known, J1357.2 has the distinction of exhibiting two quite unique properties never seen before – variable frequency dipping and a hot disc wind. We therefore re-examine the fundamentals of J1357.2:

(i) **Orbital period.** This was determined by CS13 from their outburst spectroscopy to be $2.8 \pm 0.3\text{hr}$, using $H\alpha$ emission radial velocities, making it one of the two shortest-period BH XRTs known. Normally we would expect the period to be confirmed in other ways, usually via optical or X-ray light-curves, especially if the inclination is thought to be high. However, as yet, no additional periodic variation has been seen at any wavelength, save the fast optical absorption dips (and seen only once in X-rays, AP14a). Nevertheless, the $H\alpha$ double-peak separation of 1790 km s^{-1} led CS13 to use the [Orosz & Bailyn \(1995\)](#) relation between outer disc velocity and K_2 to infer $K_2 \geq 690 \text{ km s}^{-1}$. Furthermore, this is independently supported by the [Casares \(2015\)](#) relation between $H\alpha$ FWHM and K_2 which gives $K_2 = 760 \text{ km s}^{-1}$, so these values are all self-consistent with those expected for a very low-mass donor orbiting a BH with a 2.8 hr period and indicate $f(M) > 6M_\odot$. But a direct observational confirmation of this period is still highly desirable.

(ii) **Distance.** The presence on the DSS of a faint ($r \sim 22$), very red star, led [Rau et al. \(2011\)](#) to identify this as the quiescent donor, an $\sim M4$ star at $d \sim 1.5\text{kpc}$. Such a relatively close location was not unexpected given its very high ($b \sim 50^\circ$) galactic latitude, but this implied only $L_X \sim 10^{35} \text{ erg s}^{-1}$ at outburst peak, making it a member of the class of “very faint X-ray transients” (or VFXTs). Its X-ray spectral properties (AP13) were consistent, as it remained in the hard state at maximum, but J1357.2 would then be the only BH VFXT! Nevertheless, once in quiescence, even at the DSS magnitude, it was an attractive target for VLT spectroscopy, as the short P_{orb} and BH candidature imply a high K_2 which should be straightforward to measure. This was attempted by [Torres et al. \(2015\)](#), but their spectrum was essentially identical to that seen in outburst, revealing no donor star features. More recently, the $\sim 6\text{-yr}$ OIR light-curve of J1357.2 ([Russell et al. 2018](#)) showed sustained strong variability over the $V \sim 20-22$ range outside outburst, indicative of a substantial and continuing disc-emitting component. Accordingly, with no evidence for the donor on archival surveys, support for the 1.5kpc distance disappears. This was also discussed by [Shahbaz et al. \(2013\)](#), who used the outburst amplitude - P_{orb} relation to extend the possible distance range out to $\geq 6.3\text{kpc}$, thereby increasing all the luminosity estimates by $\sim \times 40$ to at least $L_X \sim 4 \times 10^{36} \text{ erg s}^{-1}$, and hence it is *not* a VFXT.

(iii) **Inclination.** While a range of inclinations has been considered for J1357.2, (see also P19), we believe the presence of the variable frequency optical dips argues very strongly for a high inclination. Both CS13 and AP14a interpret J1357.2 as an Accretion Disc Corona (ADC) source, in which i is so high ($> 80^\circ$) that the central X-ray-emitting region is not directly visible. Instead, only X-rays scattered from the surrounding corona are observable, inferring an intrinsic L_X at least two orders of magnitude greater (see [Charles 2011](#) and references therein). It had already been noted that the X-ray to optical flux ratio of J1357.2 was low, and this is confirmed by comparison with the similar short-period, high-latitude XRT, Swift J1753.5-0127. Simultaneous X-ray/optical flux data were taken of both in outburst by Swift, giving a de-reddened $F_X/F_{UVopt} \sim 0.3$ for J1357.2 ([Beri et al. 2019](#)), but ~ 150 for Swift J1753.5-0127 ([Shaw et al. 2019](#)), i.e. ~ 500 times greater, as expected if J1357.2 is an ADC source. Curiously, the well-known

ADC sources (such as 2A1822-371, M15/AC211 and 4U2129+47) are demonstrably NS systems, which would make J1357.2 the first BH example. The key argument against the ADC interpretation is that all established ADC sources show extensive partial optical and X-ray eclipses, whereas J1357.2 shows none. However, CS13 pointed out that the very short P_{orb} of J1357.2 would require a donor mass $\leq 0.2 M_{\odot}$ which would be entirely shadowed by the disc rim, and therefore unable to produce any X-ray eclipse. The donor would of course eclipse the disc itself, but the disc variability is so great as to likely render the eclipse unobservable. Furthermore, Mata Sánchez et al. (2015) point out that the deep absorption core in HeI $\lambda 5876$ also indicates a high i ($> 75^\circ$ when observed in CVs).

4.1 What drives the outflow?

Disc winds can be driven by thermal pressure, radiation pressure or magnetic fields (e.g. Proga 2007). It is difficult to draw robust conclusions about the driving mechanism in J1357.2, but we provide a brief discussion. We adopt a BH mass of $10 M_{\odot}$ and $L_{Edd} \sim 10^{39} \text{ erg s}^{-1}$, typical values for BH XRTs (see e.g. Özel et al. 2010).

Thermal winds are caused by the X-ray corona heating the disc surface, causing the sound-speed in the irradiated disc to exceed the escape velocity (Begelman et al. 1983). It has been suggested that the equatorial disc winds observed in X-ray binaries such as GRO J1655-40 and H1743-322 can be explained by thermal and thermal-radiative driving (Higginbottom et al. 2018; Done et al. 2018; Tomaru et al. 2019). The Compton radius $R_C \approx 2 \times 10^{11} T_C^{-1} \text{ cm}$, where T_C is the Compton temperature in units of 10^8 K , which is comparable to the Compton temperature for an $\alpha = 0.8$ power-law. The critical luminosity is $L_{\text{crit}} \approx 0.03 T_C^{-1/2} L_{Edd}$. The association of the outflow with the dipping period suggests a launch radius of $\sim 2 \times 10^{10} \text{ cm}$, less than R_C but close to the critical value of $0.2 R_C$ discussed by, e.g., Done et al. (2018). Thus thermal winds may just be feasible if $L_X \gtrsim 10^{37} \text{ erg s}^{-1}$. However, the outflowing material in thermal winds tends to stay close to T_C , whereas we expect the He II absorbing material to have temperatures $\sim 40,000 \text{ K}$. We note that our inferred launch radius has an escape velocity comparable to our observed terminal velocity (see also JI19).

Radiative driving can be mediated by different opacity sources. At luminosities significantly below L_{Edd} , additional opacity sources involving bound-free or line transitions are needed to provide the necessary force. The effect is normally quantified in terms of the ‘force multiplier’, \mathcal{M} , the factor by which the radiation force is enhanced above the Thomson scattering value. Given their hard spectra relative to AGN and CVs, line-driven winds are not usually invoked in X-ray binaries. However, Tomaru et al. (2019) have shown that line and bound-free opacity might supplement thermal driving, while photoionization calculations (Dannen et al. 2018) produce $\mathcal{M} \sim 10$ for $\xi \sim 100$ plasmas with significant He II opacity. Comparison with L_{Edd} suggests that radiative driving might be possible for $L_{\text{bol}} \sim 10^{38} \text{ erg s}^{-1}$. Such a ‘boost’ from line-driving seems reasonable given the presence of absorption lines, but it still requires an extremely high intrinsic luminosity. Given the apparent difficulties with radiative and thermal driving mechanisms, it is tempting to invoke driving from either magneto-centrifugal effects (Blandford & Payne 1982) or magnetic pressure (e.g. Stone & Norman 1994). Alternatively, if the luminosity is indeed quite low, the outflow may originate in a radiatively inefficient, low accretion rate flow (Blandford & Begelman 1999). At this stage, known driving mechanisms (thermal or radiative) are only feasible for an intrinsic luminosity higher than that implied for a $d \sim 6 \text{ kpc}$. A higher

intrinsic luminosity might therefore be explained by an even larger distance and/or an extremely high inclination, and could bring the X-ray to optical flux ratio in line with canonical values for X-ray binaries. However, the source still remains puzzling in terms of its location in the radio-X-ray plane. Plotkin et al. (2016) showed the source is radio sub-luminous relative to other BH binaries, and our proposed scenario reinforces this.

ACKNOWLEDGEMENTS

We thank the anonymous referee for their constructive comments. This work is part of the SALT Large Programme 2016-2-LSP-001 (PI: Buckley). DAHB acknowledges support from the National Research Foundation. We thank T. Muñoz-Darias and F. Jiménez Ibarra for sharing their GTC results. We also thank R. Fender, S. Motta, J. Bright, N. Degenaar, S. Sim, K. Long, C. Knigge and N. Higginbottom for discussions. PAC acknowledges the Leverhulme Trust for an Emeritus Fellowship. JM is funded by STFC grant ST/N000919/1. We gratefully acknowledge the use of matplotlib (Hunter 2007). PG and JAP thank STFC and a UGC/UKIERI Thematic Partnership.

REFERENCES

Armas Padilla M., et al. 2014, *MNRAS*, 444, 902
 Begelman M. C., McKee C. F., Shields G. A., 1983, *ApJ*, 271, 70
 Beri A., et al., 2019, *MNRAS*, 485, 3064
 Blandford R. D., Begelman M. C., 1999, *MNRAS*, 303, L1
 Blandford R. D., Payne D. G., 1982, *MNRAS*, 199, 883
 Casares J., 2015, *ApJ*, 808, 80
 Casares J., Jonker P. G., 2014, *Space Science Reviews*, 183, 223
 Casares J., Charles P. A., Jones D. H. P., Rutten R. G. M., Callanan P. J., 1991, *MNRAS*, 250, 712
 Charles P., 2011, Evolution of Compact Binaries, 447, 19
 Charles P. A., Coe M. J., 2006, Compact stellar X-ray sources, 39, 215
 Corral-Santana J. M., Casares J., Muñoz-Darias T., Rodríguez-Gil P., Shahbaz T., Torres M. A. P., Zurita C., Tyndall A. A., 2013, *Science*, 339, 1048, CS13
 Corral-Santana J. M., Casares J., Muñoz-Darias T., Bauer F. E., Martínez-Pais I. G., Russell D. M., 2016, *A&A*, 587, A61
 Crawford S. M., et al., 2010, *Observatory Operations: Strategies, Processes, and Systems III*, 7737, 773725
 Dannen R. C., Proga D., Kallman T. R., Waters T., 2018, arXiv e-prints, p. arXiv:1812.01773
 Dessart L., et al., 2008, *ApJ*, 675, 644
 Done C., Tomaru R., Takahashi T., 2018, *MNRAS*, 473, 838
 Drake A. J., et al. 2017, The Astronomer’s Telegram, 10297, 1
 Hamuy M., Suntzeff N. B., Heathcote S. R., Walker A. R., Gigoux P., Phillips M. M., 1994, *PASP*, 106, 566
 Higginbottom N., Knigge C., Long K. S., Sim S. A., Matthews J. H., 2013, *MNRAS*, 436, 1390
 Higginbottom N., Knigge C., Long K. S., Matthews J. H., Sim S. A., Hewitt H. A., 2018, *MNRAS*, 479, 3651
 Hoare M. G., 1994, *MNRAS*, 267, 153
 Homer L., Charles P. A., Hakala P., Muhli P., Shih I. C., Smale A. P., Ramsay G., 2001, *MNRAS*, 322, 827
 Hunter J. D., 2007, *Computing in Science & Engineering*, 9, 90
 Jiménez-Ibarra F., Muñoz-Darias T., Casares J., Armas Padilla M., Corral-Santana J. M., 2019, *MNRAS*, in press, JI19
 Kafka S., Honeycutt R. K., 2004, *The Astronomical Journal*, 128, 2420
 Kromer M., Sim S. A., 2009, *MNRAS*, 398, 1809
 Long K. S., Knigge C., 2002, *ApJ*, 579, 725
 Long K. S., et al., 1991, *ApJ*, 381, L25
 Lucy L. B., 2002, *Astronomy and Astrophysics*, 384, 725
 Lucy L. B., 2003, *Astronomy and Astrophysics*, 403, 261
 Mata Sánchez D., Muñoz-Darias T., Casares J., Corral-Santana J. M., Shahbaz T., 2015, *MNRAS*, 454, 2199

Mata Sánchez D., et al., 2018, *MNRAS*, 481, 2646

Matthews J. H., 2016, *Ph.D. thesis, Univ. of Southampton*

Matthews J. H., Knigge C., Long K. S., Sim S. A., Higginbottom N., 2015, *MNRAS*, 450, 3331

Muñoz-Darias T., et al., 2017, *MNRAS*, 465, L124

Muñoz-Darias T., et al., 2019, *ApJ*, 879, L4

Muñoz-Darias T., et al., 2016, *Nature*, 534, 75

Muñoz-Darias T., Torres M. A. P., Garcia M. R., 2018, *MNRAS*, 479, 3987

Orosz J. A., Bailyn C. D., 1995, *ApJ*, 446, L59

Özel F., Psaltis D., Narayan R., McClintock J. E., 2010, *ApJ*, 725, 1918

Paice J. A., et al., 2019, *MNRAS*, pp 1541, P19

Plotkin R. M., et al., 2016, *MNRAS*, 456, 2707

Ponti G., Fender R. P., Begelman M. C., Dunn R. J. H., Neilsen J., Coriat M., 2012, *MNRAS*, 422, L11

Proga D., 2007, in Ho L. C., Wang J. W., eds, ASPC Vol. 373, The Central Engine of Active Galactic Nuclei. p. 267 ([arXiv:astro-ph/0701100](https://arxiv.org/abs/astro-ph/0701100))

Puls J., et al., 1996, *Astronomy and Astrophysics*, 305, 171

Quimby R. M., Wheeler J. C., Höflich P., Akerlof C. W., Brown P. J., Rykoff E. S., 2007, *ApJ*, 666, 1093

Rau A., Greiner J., Filgas R., 2011, *The Astronomer's Telegram*, 3140, 1

Russell D. M., Qasim A. A., Bernardini F., Plotkin R. M., Lewis F., Koljonen K. I. I., Yang Y.-J., 2018, *ApJ*, 852, 90

Shahbaz T., Russell D. M., Zurita C., Casares J., Corral-Santana J. M., Dhillon V. S., Marsh T. R., 2013, *MNRAS*, 434, 2696

Shaw A. W., Tetarenko B. E., Dubus G., Dinçer T., Tomsick J. A., Gandhi P., Plotkin R. M., Russell D. M., 2019, *MNRAS*, 482, 1840

Sim S. A., Drew J. E., Long K. S., 2005, *MNRAS*, 363, 615

Stone J. M., Norman M. L., 1994, *ApJ*, 433, 746

Tetarenko B. E., Sivakoff G. R., Heinke C. O., Gladstone J. C., 2016, *ApJS*, 222, 15

Tetarenko B. E., Dubus G., Lasota J. P., Heinke C. O., Sivakoff G. R., 2018, *MNRAS*, 480, 2

Tody D., 1986, *Proc. SPIE*, 627, 733

Tomaru R., Done C., Ohsuga K., Nomura M., Takahashi T., 2019, arXiv e-prints, p. arXiv:1905.11763

Torres M. A. P., Jonker P. G., Miller-Jones J. C. A., Steeghs D., Repetto S., Wu J., 2015, *MNRAS*, 450, 4292

Van Dokkum P. G., 2001, *PASP*, 113, 1420

Walborn N., Fitzpatrick E. L., 1990, *PASP*, 102, 1094

Wesemael F., Greenstein J. L., Liebert J., Lamontagne R., Fontaine G., Bergeron P., Glaspey J. W., 1993, *PASP*, 105, 761

This paper has been typeset from a $\text{\TeX}/\text{\LaTeX}$ file prepared by the author.